

University of Kentucky  
UKnowledge

Physics and Astronomy Faculty Publications

Physics and Astronomy

4-25-2016

# Ground-State Tuning of Metal-Insulator Transition by Compositional Variations in $\text{BaIr}_{1-x}\text{Ru}_x\text{O}_3$ ( $0 \leq x \leq 1$ )

Shujuan Yuan

University of Kentucky, [shujuan.yuan@uky.edu](mailto:shujuan.yuan@uky.edu)

Kamal H. Butrouna

University of Kentucky, [kamal.but@uky.edu](mailto:kamal.but@uky.edu)

Jsaminka Terzic

University of Kentucky, [jasminka.terzic@uky.edu](mailto:jasminka.terzic@uky.edu)

Hao Zheng

University of Kentucky, [hao.zheng@uky.edu](mailto:hao.zheng@uky.edu)

Saicharan Aswartham

University of Kentucky, [s.aswartham@uky.edu](mailto:s.aswartham@uky.edu)*See next page for additional authors***Click here to let us know how access to this document benefits you.**Follow this and additional works at: [https://uknowledge.uky.edu/physastron\\_facpub](https://uknowledge.uky.edu/physastron_facpub) Part of the [Condensed Matter Physics Commons](#)

## Repository Citation

Yuan, Shujuan; Butrouna, Kamal H.; Terzic, Jsaminka; Zheng, Hao; Aswartham, Saicharan; DeLong, Lance E.; Ye, Feng; Schlottmann, P.; and Cao, Gang, "Ground-State Tuning of Metal-Insulator Transition by Compositional Variations in  $\text{BaIr}_{1-x}\text{Ru}_x\text{O}_3$  ( $0 \leq x \leq 1$ )" (2016). *Physics and Astronomy Faculty Publications*. 445.  
[https://uknowledge.uky.edu/physastron\\_facpub/445](https://uknowledge.uky.edu/physastron_facpub/445)

This Article is brought to you for free and open access by the Physics and Astronomy at UKnowledge. It has been accepted for inclusion in Physics and Astronomy Faculty Publications by an authorized administrator of UKnowledge. For more information, please contact [UKnowledge@lsv.uky.edu](mailto:UKnowledge@lsv.uky.edu).

---

**Authors**

Shujuan Yuan, Kamal H. Butrouna, Jsaminka Terzic, Hao Zheng, Saicharan Aswartham, Lance E. DeLong, Feng Ye, P. Schlottmann, and Gang Cao

**Ground-State Tuning of Metal-Insulator Transition by Compositional Variations in  $\text{BaIr}_{1-x}\text{Ru}_x\text{O}_3$  ( $0 \leq x \leq 1$ )****Notes/Citation Information**

Published in *Physical Review B*, v. 93, issue 16, 165136, p. 1-5.

©2016 American Physical Society

The copyright holder has granted permission for posting the article here.

**Digital Object Identifier (DOI)**

<https://doi.org/10.1103/PhysRevB.93.165136>

# Ground-state tuning of metal-insulator transition by compositional variations in $\text{BaIr}_{1-x}\text{Ru}_x\text{O}_3$ ( $0 \leq x \leq 1$ )

S. J. Yuan,<sup>1,\*</sup> K. Butrouna,<sup>1</sup> J. Terzic,<sup>1</sup> H. Zheng,<sup>1</sup> S. Aswartham,<sup>1</sup> L. E. DeLong,<sup>1</sup> Feng Ye,<sup>2</sup> P. Schlottmann,<sup>3</sup> and G. Cao<sup>1,†</sup><sup>1</sup>*Department of Physics and Astronomy, Center for Advanced Materials, University of Kentucky, Lexington, Kentucky 40506, USA*<sup>2</sup>*Quantum Condensed Matter Division, Oak Ridge National Laboratory, Oak Ridge, Tennessee 37831, USA*<sup>3</sup>*Department of Physics, Florida State University, Tallahassee, Florida 32306, USA*

(Received 9 October 2015; revised manuscript received 23 March 2016; published 25 April 2016)

Hexagonal  $\text{BaIrO}_3$  is a magnetic insulator driven by the spin-orbit interaction (SOI), whereas  $\text{BaRuO}_3$  is an enhanced paramagnetic metal. Our investigation of structural, magnetic, transport, and thermal properties reveals that substitution of  $\text{Ru}^{4+}$  ( $4d^4$ ) ions for  $\text{Ir}^{4+}$  ( $5d^5$ ) ions in  $\text{BaIrO}_3$  reduces the magnitudes of the SOI and a monoclinic structural distortion and rebalances the competition between the SOI and the lattice degrees of freedom to render an evolution from a magnetic insulating state to a robust metallic state. The central findings of this paper are as follows: (1) light Ru doping ( $0 < x \leq 0.15$ ) prompts simultaneous, precipitous drops in both the magnetic ordering temperature  $T_N$  and the electrical resistivity, and (2) heavier Ru doping ( $0.41 \leq x \leq 0.9$ ) induces a robust metallic state without any long-range magnetic order. All results suggest a critical role of the lattice degrees of freedom in determining the ground state in the heavy transition-metal oxides.

DOI: [10.1103/PhysRevB.93.165136](https://doi.org/10.1103/PhysRevB.93.165136)

## I. INTRODUCTION

A unique feature of the  $5d$  iridates is that a strong spin-orbit interaction (SOI) competes vigorously with Coulomb interactions, noncubic crystalline electric fields, and Hund's rule coupling [1–5]. The relative strengths of these interactions stabilize new exotic ground states that provide a fertile ground for studying new physics. In particular, it is now recognized that strong SOI can drive novel narrow-gap Mott insulating states in iridates. The SOI is a relativistic effect that is proportional to  $Z^2$  ( $Z$  is the atomic number), is approximately 0.4 eV in the iridates (compared to  $\sim 20$  meV in  $3d$  materials), and splits the  $t_{2g}$  bands into states with  $J_{\text{eff}} = 1/2$  and  $J_{\text{eff}} = 3/2$ , the latter having lower energy. Since the  $\text{Ir}^{4+}$  ( $5d^5$ ) ions provide five  $5d$  valence electrons, four of them fill the lower  $J_{\text{eff}} = 3/2$  bands, and one electron partially occupies the  $J_{\text{eff}} = 1/2$  band in which the Fermi level  $E_F$  resides. The  $J_{\text{eff}} = 1/2$  band is so narrow that even a reduced  $U$  ( $\sim 0.50$  eV due to the extended nature of  $5d$ -electron orbitals) is sufficient to open a gap ( $\leq 0.62$  eV) that induces a novel insulating state, which is contrary to expectations based upon the relatively large unsplit  $5d$  bandwidth [1–3,6].

Adopting a distorted hexagonal structure with both face-sharing and corner-sharing  $\text{IrO}_6$  octahedra,  $\text{BaIrO}_3$  is particularly unique in that it exhibits a simultaneous onset of weak ferromagnetic transition due to a canted antiferromagnetic structure and charge-density wave (CDW) orders with Néel temperature  $T_N = 183$  K, comparable to that of other iridates, such as 240 K for  $\text{Sr}_2\text{IrO}_4$  [7] and 285 K for  $\text{Sr}_3\text{Ir}_2\text{O}_7$  [8], and a temperature-driven transition from a bad metal to an insulating ground state [9–11]. The ground state of  $\text{BaIrO}_3$  is extremely sensitive to lattice contractions that can be tuned by light doping or the application of hydrostatic pressures [4,12,13]. The extraordinary delicacy of the ground state in  $\text{BaIrO}_3$  implies a critical balance among orbital, electronic, and lattice

degrees of freedom [4,14]. The hexagonal structure of  $\text{BaIrO}_3$  is similar to that of nine-layered rhombohedral  $\text{BaRuO}_3$ , which exhibits a crossover from metallic to insulating behavior and enhanced paramagnetism with decreasing temperature [15,16]. However, a monoclinic distortion extant in  $\text{BaIrO}_3$  at room temperature and 90 K generates twisting and buckling of the cluster trimers (see Fig. 1) that give rise to two one-dimensional (1D) zigzag chains along the  $c$  axis and a two-dimensional layer of corner-sharing  $\text{IrO}_6$  octahedra on the  $ab$  plane [9,12,17–19].

Although  $\text{BaIrO}_3$  and  $\text{BaRuO}_3$  have similar structures, they exhibit sharply contrasting physical properties, which underscore the critical role SOI ( $\sim 0.4$  eV for iridates and  $\sim 0.15$  eV for ruthenates) [3], and the lattice degrees of freedom can play in determining the ground state in iridates. In this paper, substituting  $\text{Ru}^{4+}$  ( $4d^4$ ) for  $\text{Ir}^{4+}$  ( $5d^5$ ) in single-crystal  $\text{BaIr}_{1-x}\text{Ru}_x\text{O}_3$  ( $0 \leq x \leq 1$ ) reduces the magnitude of the SOI, the structural distortions, and adds holes to the  $t_{2g}$  bands. The overall effect of Ru doping is to lower  $E_F$  and move the system away from the Mott instability toward a more robust metallic state. The emerging metallic state with delocalized electrons also accompanies a decrease in  $T_N$ .

## II. EXPERIMENT

The single crystals of  $\text{BaIr}_{1-x}\text{Ru}_x\text{O}_3$  were grown by conventional flux methods similar to earlier reports [9,15] using  $\text{BaCl}_2$  as a self-flux. Crystals were grown in platinum crucibles using  $\text{IrO}_2$  (99.98%, Alfa Aesar),  $\text{RuO}_2$  (99.98%, Alfa Aesar),  $\text{BaCO}_3$  (99.99%, Alfa Aesar), and anhydrous  $\text{BaCl}_2$  (99.5%, Alfa Aesar). Starting powders were placed in a Pt crucible with a Pt lid, and this assembly was then put in an alumina crucible with a cover. The mixtures were heated up to 1480 °C and then cooled to 1350 °C at a rate of 5 °C per hour before cooling down to room temperature. The ratio of the sample to flux remains at 1:8 throughout the entire series of  $\text{BaIr}_{1-x}\text{Ru}_x\text{O}_3$ . The crystals have a hexagonal surface and a visible layered texture along the  $c$  axis as

\*Corresponding author: [sjyuan.shu@gmail.com](mailto:sjyuan.shu@gmail.com)†[cao@uky.edu](mailto:cao@uky.edu)

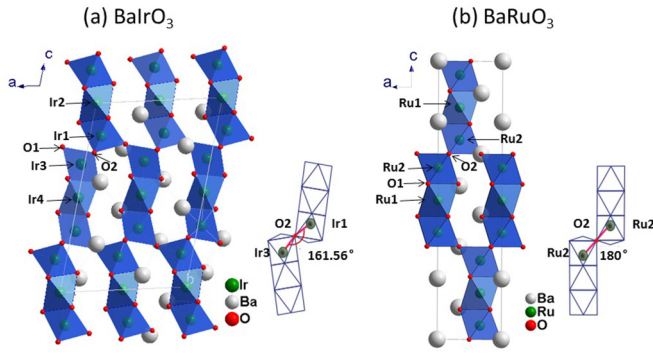


FIG. 1. Comparison of the nine-layer crystallographic form (a)  $\text{BaIrO}_3$  and (b)  $\text{BaRuO}_3$  crystal structure. Note the corner-sharing  $\text{Ir}_3\text{O}_{12}$  and  $\text{Ru}_3\text{O}_{12}$  trimers that are connected through the vertices of the top and bottom octahedra of the trimers and the schematic of the  $M\text{-O}_2\text{-}M$  bond angle  $\theta$  ( $M = \text{Ir}$  or  $\text{Ru}$ ).

shown in the inset of Fig. 2(a). The crystal structures were determined using a Nonius Kappa CCD x-ray diffractometer or a Rigaku x-ray diffractometer XtaLAB PRO equipped with a PILATUS 200-K hybrid pixel array detector at 90 or 240 K, and they were refined by full matrix least squares using the SHELX-97 programs [20]. The standard deviations of all lattice parameters and interatomic distances are smaller than 0.1%. The atomic parameters for  $\text{BaIr}_{1-x}\text{Ru}_x\text{O}_3$  are available in the Supplemental Material [21]. Chemical compositions of the single crystals were estimated using a combined unit of

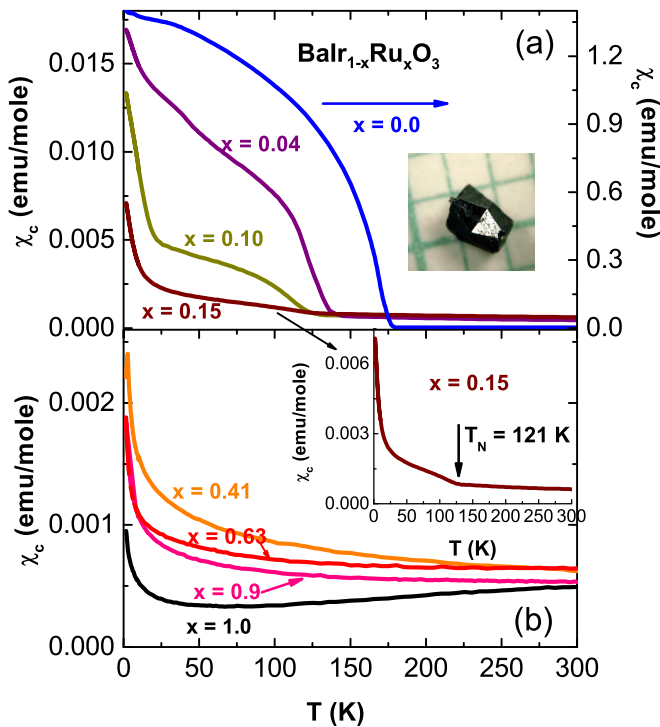


FIG. 2. The magnetic susceptibilities  $\chi(T)$  along the  $c$  axis for  $\text{BaIr}_{1-x}\text{Ru}_x\text{O}_3$  where (a)  $0 \leq x \leq 0.15$  and (b)  $0.42 \leq x \leq 1$ . The data were collected after a field cooling procedure at  $\mu_0 H = 0.1$  T. The inset in (a) shows a representative single crystal of  $\text{BaIr}_{1-x}\text{Ru}_x\text{O}_3$  with  $x = 0$ . The inset in (b) shows an enlarged  $\chi_c(T)$  for  $x = 0.15$ .

Hitachi/Oxford SwiftED 3000 for energy dispersive x-ray spectroscopy. The magnetization  $M(T)$ , electrical resistivity  $\rho(T)$ , and specific heat  $C(T)$  were measured between 1.7 and 400 K using a Quantum Design 7T superconducting quantum interference device (SQUID) magnetometer and a Quantum Design 9T physical property measurement system, respectively.

### III. RESULTS AND DISCUSSION

The two end members  $\text{BaIrO}_3$  and  $\text{BaRuO}_3$  both have nine-layer rhombohedral phases with different space groups as shown in Figs. 1(a) and 1(b). The  $C2/m(12)$  space group of  $\text{BaIrO}_3$  features three face-sharing  $\text{IrO}_6$  octahedra forming  $\text{Ir}_3\text{O}_{12}$  trimers that are corner and face shared via  $\text{IrO}_6$  octahedra (containing  $\text{Ir}_1$  and  $\text{Ir}_3$  sites) to form 1D chains along the  $c$  axis [12,16–19] [see Fig. 1(a)]. A monoclinic distortion generates twisting and buckling of the trimers (tilted  $\sim 12^\circ$  relative to each other), which gives rise to two 1D zigzag chains along the  $c$  axis and a two-dimensional layer of corner-sharing  $\text{IrO}_6$  octahedra on the  $ab$  plane. Substituting  $\text{Ru}^{4+}$  for  $\text{Ir}^{4+}$  preserves the monoclinic structure in the entire doping range ( $x \leq 0.90$ ) except for  $x = 1$  as shown in Table I. It results in a nearly uniform reduction in lattice parameters  $a$ - $c$  axes and the unit-cell volume  $V$ . This behavior is expected because the ionic radius of  $\text{Ru}^{4+}$  (0.620 Å) is slightly smaller than that of  $\text{Ir}^{4+}$  (0.625 Å). In addition, the  $\text{Ir/Ru-O-Ir/Ru}$  bond angle  $\theta$  increases linearly with increasing Ru concentration  $x$  and eventually reaches  $180^\circ$  for  $x = 1$  (i.e.,  $\text{BaRuO}_3$ ), indicating a significantly less distorted lattice.  $\text{BaRuO}_3$  or  $x = 1$  exhibits a similar crystal structure with the  $R\bar{3}m(166)$  space group as shown in Fig. 1(b). Three  $\text{RuO}_6$  octahedra share faces in a partial chain, facilitating direct Ru-Ru  $d$ -orbital interactions between the octahedra. Each of these triple units or trimers of the octahedra shares corners with its neighbors along the hexagonal axis via nearly  $180^\circ$  bond angles that favor superexchange coupling [Fig. 1(b)].

Ru doping induces pronounced changes in a wide range of physical properties of single-crystal  $\text{BaIr}_{1-x}\text{Ru}_x\text{O}_3$ . Representative data for the  $c$ -axis magnetic susceptibility  $\chi_c(T)$  that shows the weak magnetic transition at  $T_N$  is depressed from 183 K for  $x = 0$  to 145 K for  $x = 0.04$  and vanishes for  $x \geq 0.41$  is presented in Fig. 2.

The magnetic anisotropy also decreases with Ru additions as shown in Fig. 3. Magnetic anisotropy is in general a result of SOI; Ru doping weakens the SOI, therefore, leading to a smaller magnetic anisotropy. Furthermore, Hund's rule coupling competes with the SOI and thus weakens the relative strength of the SOI. With increasing  $x$ , the  $c$ -axis susceptibility  $\chi_c(T)$  becomes relatively stronger and larger than the basal-plane susceptibility  $\chi_{ab}(T)$  [see Figs. 3(b) and 3(c)]. This change suggests a spin flop from the basal plane to the  $c$  axis due to Ru doping. For  $x = 1$ , the basal-plane  $\chi_{ab}(T)$  is larger than  $\chi_c(T)$  again [see Fig. 3(d)]. Similar phenomena were also observed in  $\text{Ca}_2\text{Ru}_{1-x}\text{Ir}_x\text{O}_4$  [22] and  $\text{Sr}_2\text{Ir}_{1-x}\text{Ru}_x\text{O}_4$  [23]. This behavior could be due to the strong interaction between Ru  $4d$  and Ir  $5d$  electrons.

It is already established that the bond angle  $\theta$  is critical to the electronic and magnetic structures of iridates [4]. As shown in Fig. 4(a),  $\theta$  increases linearly with increasing  $x$  and

TABLE I. The crystal structure and refinement details of  $\text{BaIr}_{1-x}\text{Ru}_x\text{O}_3$  at 90 K for  $x = 0, 0.10, 0.63$ , and 1 and at 240 K for  $x = 0.82$  and 0.90. The diffractometer is a Nonius Kappa CCD, and the absorption correction is a multiscan SADABS. The Ir/Ru-O<sub>2</sub>-Ir/Ru bond angle is defined in Fig. 1.

	$x = 0$ (90 K)	$x = 0.10$ (90 K)	$x = 0.63$ (90 K)	$x = 0.82$ (240 K)	$x = 0.90$ (240 K)	$x = 1$ (90 K)
Crystal system, space group	Monoclinic, $C12/m1(12)$	Monoclinic, $C12/m1(12)$	Monoclinic, $C12/m1(12)$	Monoclinic, $C12/m1(12)$	Monoclinic, $C12/m1(12)$	Trigonal, $R\bar{3}m(166)$
$a$ - $c$ (Å)	$a = 9.9935(2),$ $b = 5.7352(1),$ $c = 15.2376(3)$	$a = 9.9839(2),$ $b = 5.7377(1),$ $c = 15.1107(4)$	$a = 9.9440(2),$ $b = 5.7429(1),$ $c = 14.8102(4)$	$a = 9.9999(5),$ $b = 5.7759(4),$ $c = 14.8916(4)$	$a = 9.9923(4),$ $b = 5.7733(3),$ $c = 14.8882(8)$	$a = 5.7366(1),$ $c = 21.5933(6)$
$\beta$ (deg)	103.411(1)	103.3402(9)	102.8574(9)	102.939(5)	102.882(4)	NA
$V$ (Å <sup>3</sup> )	849.10(6)	842.25(3)	824.57(3)	838.28(8)	837.26(7)	615.40(3)
$Z$	12	12	12	12	12	9
Bond angle (deg)	161.671(1)	163.678(0)	174.296(1)	175.1(3)	176.1(1)	180.0
	Data collection					
Number of measured, independent, and observed [ $I > 4\sigma(I)$ ] reflections	6066,398,350	7075,396,369	7210,398,353	14459,1643,1525	14071,1769,1633	7256,401,398
$R_{int}$	0.021	0.031	0.035	0.027	0.038	0.025
	Refinement					
$R[F^2 > 4\sigma(F^2)],$ $wR(F^2), S$	0.016,0.035,1.05	0.02,0.049,1.15	0.025,0.069,1.17	0.067,0.1847,1.085	0.0720,205,1.024	0.02,0.035,1.09

eventually reaches an ideal 180° for  $x = 1$ . The increase in  $\theta$  directly enhances the electron hopping and favors a more metallic state with a concurrent decrease in  $T_N$  [see Fig. 4(b)].

Indeed, the evolution from the insulating to the itinerant state upon Ru doping is clearly illustrated in the electrical resistivity  $\rho(T)$ . For  $x = 0$ , both the  $ab$  plane and the  $c$  axis  $\rho_{ab}(T)$  and  $\rho_c(T)$  exhibit a sharp kink at  $T_N = 183$  K, consistent with previous results in which the energy gap is estimated to be 0.1 eV [9,17]. With Ru doping, both  $\rho_{ab}(T)$  and  $\rho_c(T)$  decrease rapidly (see Fig. 5). It is noted that the metallic

behavior at higher temperatures for  $x = 0.04$  [see Fig. 5(b)] does not seem to follow the general trend displayed by other compositions although the behavior is highly reproducible.

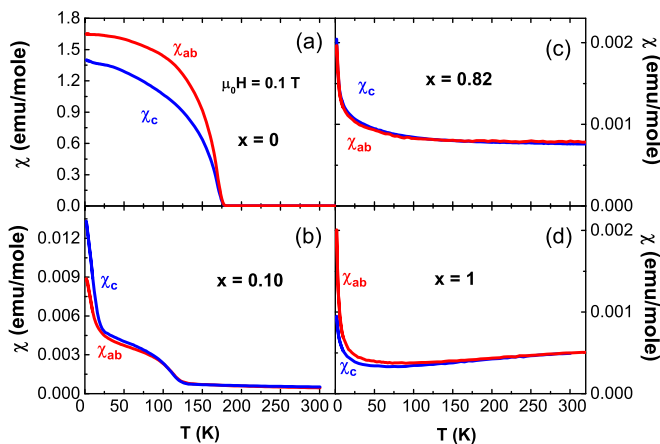


FIG. 3. The magnetic susceptibilities  $\chi(T)$  on the  $ab$  plane and along the  $c$  axis for representative compositions (a)  $x = 0$ , (b)  $x = 0.10$ , (c)  $x = 0.82$ , and (d)  $x = 1$ , respectively. The magnetization was measured after field cooling at  $\mu_0H = 0.1$  T.

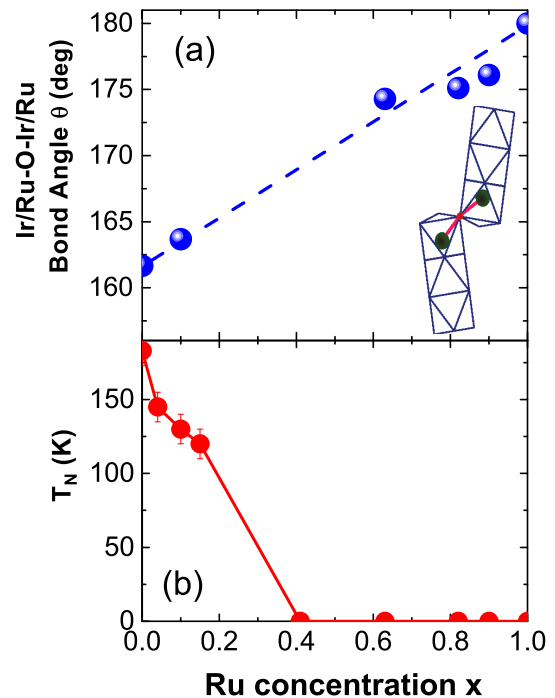


FIG. 4. The Ru concentration  $x$  dependence of (a) the Ir/Ru-O<sub>2</sub>-Ir/Ru bond angle  $\theta$  and (b)  $T_N$ . The inset: schematic of the Ir/Ru-O<sub>2</sub>-Ir/Ru bond angle  $\theta$ . Note that  $\theta$  increases linearly with increasing  $x$ .

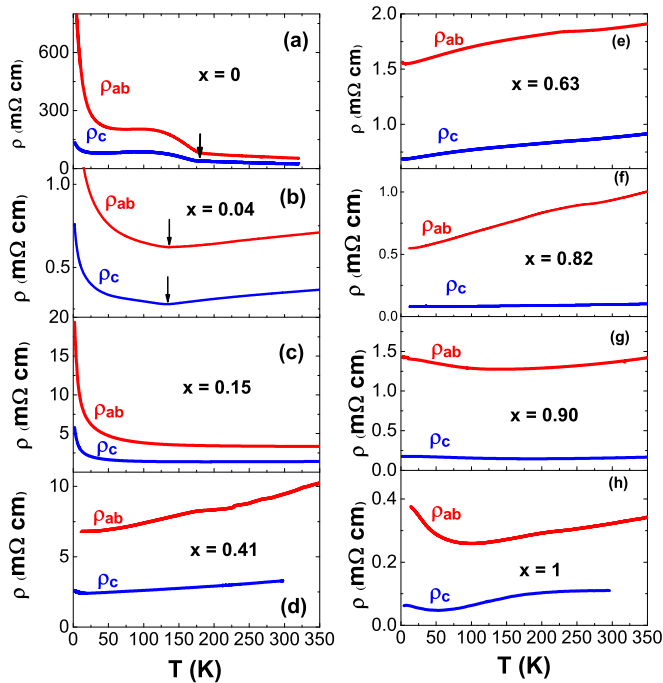


FIG. 5. The temperature dependence of the resistivity  $\rho(T)$  for representative compositions (a)  $x = 0$ , (b)  $x = 0.04$ , (c)  $x = 0.15$ , (d)  $x = 0.41$ , (e)  $x = 0.63$ , (f)  $x = 0.82$ , (g)  $x = 0.90$ , and (h)  $x = 1$ . The vertical arrows indicate the kink that corresponds to the weak magnetic transition at  $T = T_N$ .

The origin of this brief occurrence of the metallic state is yet to be understood. Nevertheless, dilute Ru substitutions for Ir result in a reduced  $\rho(T)$  and an emerging metallic state for  $x > 0.15$ . For  $x = 1$  or  $\text{BaRuO}_3$ , a broad upturn in  $\rho_{ab}(T)$  at low temperatures might be a result of a pseudogap formation and 1D-CDW fluctuations according to Ref. [16].

The temperature dependence of the specific heat  $C(T)$  for various  $x$ 's is given in Fig. 6(a). Fitting the data to  $C(T) = \gamma T + \beta T^3$  for  $7 < T < 17$  K yields the Sommerfeld coefficient  $\gamma$  for the electronic contribution to  $C(T)$  [see Fig. 6(b)], which serves as a measure of the electronic density of states at the Fermi level  $N(E_F)$  and the effective mass of the carriers. There is a substantial increase in  $\gamma$  with dilute Ru concentration; in particular,  $\gamma$  reaches  $11.75 \text{ mJ mol}^{-1} \text{ K}^{-2}$  for  $x = 0.04$  and  $15.09 \text{ mJ mol}^{-1} \text{ K}^{-2}$  for  $x = 0.15$ , compared to  $\gamma = 2.34 \text{ mJ mol}^{-1} \text{ K}^{-2}$  for the parent compound ( $x = 0.0$ ). The  $\gamma$  for  $0.04 \leq x \leq 0.15$  in which the metallic state is not fully developed is unexpectedly high, and this is likely due to spin fluctuations existent in the system. Nevertheless,  $N(E_F)$  and  $\gamma$  eventually decrease with  $x$  as shown in Fig. 6(b). In the case of  $\text{BaRuO}_3$ , the smaller values reflect pseudogap formation due to the CDW instability [16].

#### IV. CONCLUSIONS

We have investigated the structural, magnetic, transport, and thermal properties of  $\text{BaIr}_{1-x}\text{Ru}_x\text{O}_3$ . Ru doping rebalances

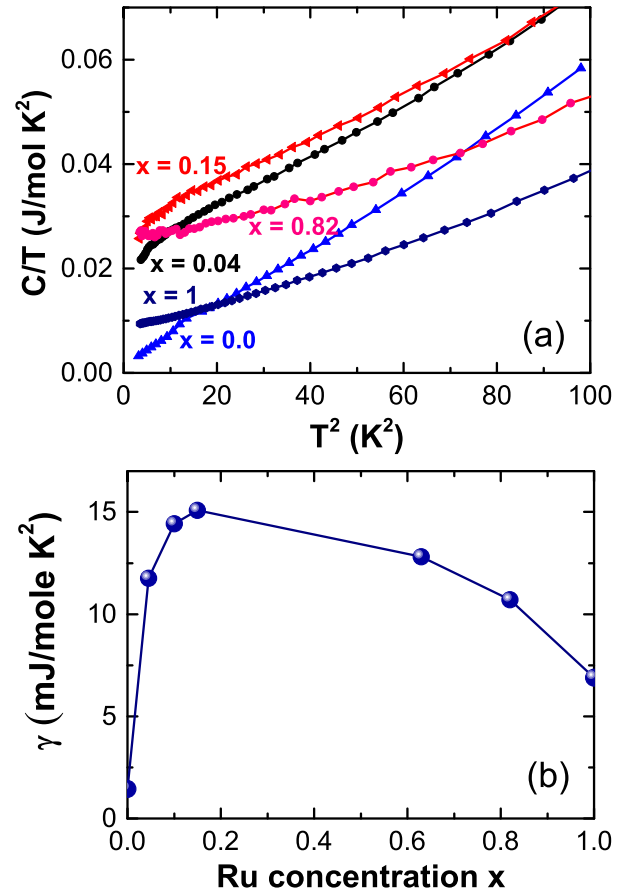


FIG. 6. (a) The specific heat  $C(T)/T$  vs  $T^2$  and (b) the Sommerfeld coefficient  $\gamma$  vs  $x$  for  $\text{BaIr}_{1-x}\text{Ru}_x\text{O}_3$ .

the competition among the SOI, electron correlations, and the lattice degrees of freedom to generate a metallic state for  $x > 0.15$ . The Ru doping alters the relative strength of the SOI that dictates the ground state, which, in turn, affects the band gap near  $E_F$ . Unlike the situation in  $\text{Sr}_2\text{IrO}_4$  that features an unconventional correlation between the magnetic transition and the charge gap, the evolution of the ground state in  $\text{BaIr}_{1-x}\text{Ru}_x\text{O}_3$  appears to indicate a strong coupling between the magnetic order and the metal-insulator transition. All results suggest the critical role of lattice degrees of freedom that, along with the SOI, dictate the ground state of the heavy transition-metal oxides.

#### ACKNOWLEDGMENTS

This work was supported by the National Science Foundation via Grant No. DMR-1265162 (G.C.) and Department of Energy (BES) through Grants No. DE-FG02-98ER45707 (P.S.) and No. DE-FG02-97ER45653 (L.E.D.).

[1] B. J. Kim, H. Jin, S. J. Moon, J. Y. Kim, B. G. Park, C. S. Leem, J. Yu, T. W. Noh, C. Kim, S. J. Oh, J. H. Park, V.

Duraij, G. Cao, and E. Rotenberg, *Phys. Rev. Lett.* **101**, 076402 (2008).

- [2] B. J. Kim, H. Ohsumi, T. Komesu, S. Sakai, T. Morita, H. Takagi, and T. Arima, *Science* **323**, 1329 (2009).
- [3] G. Cao and L. E. DeLong, in *Frontiers of 4d- and 5d-Transition Metal Oxides* (World Scientific, Singapore, 2013).
- [4] O. B. Korneta, S. Chikara, S. Parkin, L. E. DeLong, P. Schlottmann, and G. Cao, *Phys. Rev. B* **81**, 045101 (2010).
- [5] T. F. Qi, O. B. Korneta, L. Li, K. Butrouna, V. S. Cao, X. Wan, P. Schlottmann, R. K. Kaul, and G. Cao, *Phys. Rev. B* **86**, 125105 (2012).
- [6] J. Dai, E. Calleja, G. Cao, and K. McElroy, *Phys. Rev. B* **90**, 041102 (2014).
- [7] G. Cao, J. Bolivar, S. McCall, J. E. Crow, and R. P. Guertin, *Phys. Rev. B* **57**, R11039 (1998).
- [8] G. Cao, Y. Xin, C. S. Alexander, J. E. Crow, P. Schlottmann, M. K. Crawford, R. L. Harlow, and W. Marshall, *Phys. Rev. B* **66**, 214412 (2002).
- [9] G. Cao, J. E. Crow, R. P. Guertin, P. F. Henning, C. C. Homes, M. Strongin, D. N. Basov, and E. Lochner, *Solid State Commun.* **113**, 657 (2000).
- [10] M. L. Brooks, S. J. Blundell, T. Lancaster, W. Hayes, F. L. Pratt, P. P. C. Frampton, and P. D. Battle, *Phys. Rev. B* **71**, 220411 (2005).
- [11] M. A. Laguna-Marco, D. Haskel, N. Souza-Neto, J. C. Lang, V. V. Krishnamurthy, S. Chikara, G. Cao, and M. van Veenendaal, *Phys. Rev. Lett.* **105**, 216407 (2010).
- [12] G. Cao, X. N. Lin, S. Chikara, V. Durairaj, and E. Elhami, *Phys. Rev. B* **69**, 174418 (2004).
- [13] M. A. Laguna-Marco, G. Fabbris, N. M. Souza-Neto, S. Chikara, J. S. Schilling, G. Cao, and D. Haskel, *Phys. Rev. B* **90**, 014419 (2014).
- [14] W. Ju, G.-Q. Liu, and Z. Yang, *Phys. Rev. B* **87**, 075112 (2013).
- [15] M. Shepard, S. McCall, G. Cao, and J. E. Crow, *J. Appl. Phys.* **81**, 4978 (1997).
- [16] Y. S. Lee, J. S. Lee, K. W. Kim, T. W. Noh, J. Yu, Y. Bang, M. K. Lee, and C. B. Eom, *Phys. Rev. B* **64**, 165109 (2001).
- [17] A. V. Powell and P. D. Battle, *J. Alloys Compd.* **191**, 313 (1993).
- [18] M. H. Whangbo and H. J. Koo, *Solid State Commun.* **118**, 491 (2001).
- [19] R. Lindsay, W. Strange, B. L. Chamberland, and R. O. Moyer, Jr., *Solid State Commun.* **86**, 759 (1993).
- [20] G. M. Sheldrick, *Acta Cryst.* **A64**, 112 (2008).
- [21] See Supplemental Material at <http://link.aps.org/supplemental/10.1103/PhysRevB.93.165136> for substantial information on crystal refinements.
- [22] S. J. Yuan, J. Terzic, J. C. Wang, L. Li, S. Aswartham, W. H. Song, F. Ye, and G. Cao, *Phys. Rev. B* **92**, 024425 (2015).
- [23] S. J. Yuan, S. Aswartham, J. Terzic, H. Zheng, H. D. Zhao, P. Schlottmann, and G. Cao, *Phys. Rev. B* **92**, 245103 (2015).